Resonant photoemission study of the electronic structure of 3 keV nitrogen-implanted tantalum

A. Arranz,[1] C. Palacio,[1,*] and J. Avila[2]
[1]*Departamento de Física Aplicada, Facultad de Ciencias, C-XII, Universidad Autónoma de Madrid, Cantoblanco, 28049-Madrid, Spain*
[2]*LURE, Centre Universitaire Paris-Sud, Bât. 209 D, B.P. 34, 91898 Orsay Cedex, France and Instituto de Ciencia de Materiales de Madrid, CSIC, Cantoblanco, 28049-Madrid, Spain*
(Received 22 June 2004; published 7 January 2005)

The electronic properties of tantalum nitride thin films grown by 3 keV nitrogen implantation have been studied with resonant photoemission using synchrotron radiation. Resonant photoemission from the valence band was observed when the photon energy was in the neighborhood of the Ta $5p \rightarrow 5d$, $5p \rightarrow 6sp$ and $4f \rightarrow 5d$ transition energies. The constant initial state curves show multiple resonance maxima that are explained in terms of the Ta $5p \rightarrow 5d$, $5p \rightarrow 6sp$ and $4f \rightarrow 5d$ photoabsorption mechanisms, the spin-orbit splitting of the Ta $5p$ and Ta $4f$ core levels, and the splitting of the N–Ta hybridized unoccupied states by crystal-field interactions. A strong resonance has been observed at the Ta$4f \rightarrow 5d$ transition. Resonant photoemission results suggest a strong hybridization of the Ta $5d$ and N $2p$ atomic orbitals along the main feature of the VB (between $\sim$3–9 eV) due to the extended nature of Ta orbitals. Occupied vacancy states at $\sim$2 eV show a resonance enhancement that supports the Ta character recently predicted for such states by Stampfl and Freeman. Stronger resonances are found for the hybridized Ta $5d$-N $2p$ valence band features lying in the $\sim$3–9 eV range, than for the essentially Ta-like ones just below the Fermi level. This suggests that an interatomic recombination mechanism in which N $2p$ states resonate themselves could also take place.

DOI: 10.1103/PhysRevB.71.035405 PACS number(s): 81.05.Je, 71.20.−b, 79.60.−i

I. INTRODUCTION

In the last years tantalum nitride has received much attention due to its unique combination of physical and chemical properties. Specifically, tantalum nitride thin films have been used as diffusion barriers, wear and corrosion-resistance coatings and very precise and stable thin film resistors in microelectronics.[1–6] As a consequence of that, a special effort has been devoted to the synthesis and structural characterization of tantalum nitride thin films.[1–9] However, its electronic structure, a key point to control the properties of the films in many of the above-mentioned applications, has received less attention.

The electronic structure of tantalum nitride has been investigated by x-ray photoelectron spectroscopy (XPS),[4,10–12] electron energy loss spectroscopy (EELS),[13] x-ray emission spectroscopy (XES),[14] and x-ray absorption spectroscopy (XAS).[15] Moreover, several band structure calculations have been published for hexagonal and cubic TaN,[16–21] and for nonstoichiometric cubic tantalum nitrides.[20,21] However, resonant photoemission experiments, which can provide useful information about its electronic structure, have not been carried out.

Resonant photoemission in $3d$ transition metals (TM's) has been the subject of many recent experimental and theoretical investigations.[22] The phenomenon is usually explained as due to an interference effect between the direct photoemission process and autoionization of a localized excited state created by photoabsorption. It is observed when the energy of incident photons is varied around the threshold for a $p \rightarrow d$ transition. The resonance has been also found in TM's oxides where the d band is completely suppressed. In such cases, it is explained as due to the hybridization between the O $2p$ and cation d orbitals, and therefore resonant photoemission is used to isolate the d-states contribution and to study the valence band (VB) structure of TM's oxides.[22–29] Anyway, the number of works dealing with resonant photoemission on TM nitrides is rather scarce. In fact, only $3d$ and $4d$ TM nitrides have been studied by resonant photoemission.[30–33] Therefore, the aim of this work is to study the VB electronic structure of tantalum nitride by resonant photoemission to determine its cationic character. Also, information about the unoccupied electronic states has been obtained from the N K XAS spectrum.

II. EXPERIMENT

The experiments were performed at LURE (Orsay, France) using the PES2 experimental station connected to the SU8 ondulator beamline of the Super-Aco storage ring. The measurements were carried out in an ultra high vacuum system, with a base pressure better than 1×10^{-10} Torr, equipped with an angle resolving 50 mm hemispherical VSW analyzer coupled to a goniometer inside the chamber. XAS spectra were measured in the total electron yield mode. Photoemission and XAS spectra have been normalized to the incident current measured in a gold grid located at the entrance of the analysis chamber. For the photon energy range used in this work, the overall energy resolution, including the analyzer, was estimated to be better than 0.1 eV.

A tantalum foil of 99.99% purity manufactured by Reframet-Hoboken was used throughout this work. The sample was sputter-cleaned *in situ* using a 3 keV Ar^+ beam rastered over an area of 1×1 cm^2 until no impurities were detected. The tantalum nitride thin films have been grown by 5N nitrogen implantation of a tantalum substrate at room temperature using an extractor type ion gun. The ion beam

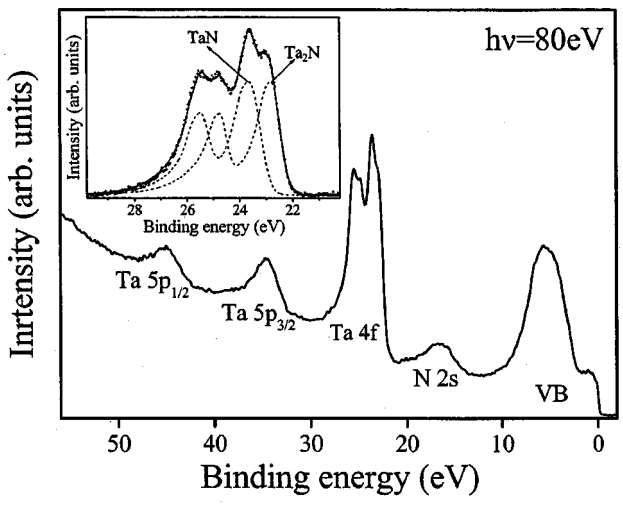

FIG. 1. Overview spectrum of a 3 keV N_2^+ implanted tantalum substrate measured at a photon energy $h\nu$=80 eV. The inset shows the deconvolution of the Ta 4*f* spectrum (dotted line) using two synthetic doublets for the Ta_2N and TaN phases (dashed lines).

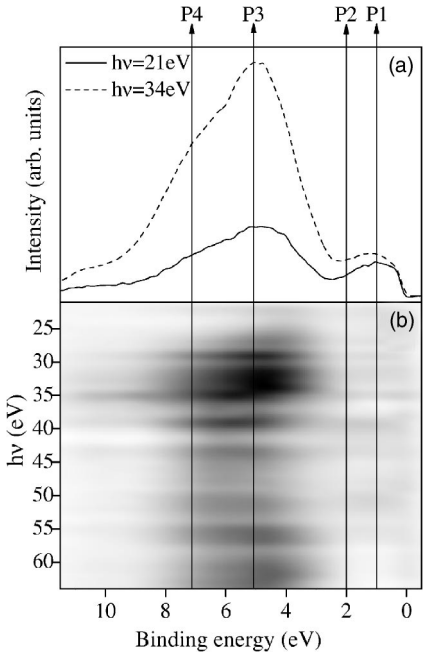

FIG. 2. (a) Comparison of the VB spectra measured at photon energies of 21 and 34 eV, and (b) intensity of the difference spectra calculated by subtraction of the spectra measured at $h\nu$=21 eV (off resonance) from all measured spectra, as a function of binding energy and photon energy. Several features are indicated by arrows.

was normal to the sample surface and was rastered over an area of 1×1 cm^2 with a current density of 10 μA/cm^2, as measured in the tantalum sample. The beam energy was 3 keV and the ion dose was in the saturation range. These experimental conditions lead to a ~90 Å thick tantalum nitride film ($TaN_{0.7}$) formed by a mixture of Ta_2N and TaN phases.[11,12]

III. RESULTS AND DISCUSSION

Figure 1 shows an overview spectrum of a 3 keV N_2^+ implanted tantalum substrate measured at a photon energy $h\nu$ =80 eV. The implantation has been carried out at room temperature up to saturation. The spectrum shows the Ta $5p_{3/2}$-$5p_{1/2}$ doublet at 34.6 and 45.1 eV, the Ta 4*f* doublet, the N 2*s* band at 16.7 eV and the VB between 10 and 0 eV. The inset of Fig. 1 shows the detailed Ta 4*f* spectrum (dotted line) after background subtraction based on a modified Shirley method.[34] Two different Ta—N contributions can be clearly distinguished at ~22.9 and 23.6 eV, respectively, and have been previously assigned to Ta_2N and TaN phases.[12] The deconvolution of the Ta 4*f* spectrum using two synthetic doublets for the Ta_2N and TaN phases (dashed lines) is also shown. It should be pointed out, that neither oxygen nor carbon 1*s* bands have been detected in the nitrogen implanted tantalum substrate using a photon energy of 640 eV.

To analyze the resonant photoemission behavior of the tantalum nitride film at the Ta 5*p* and 4*f* thresholds, a set of valence band spectra have been measured for different photon energies between 21 and 64 eV in steps of 1 eV. The total intensity and the relative intensities of the different VB features strongly depend on the photon energy due to resonance processes. As an example, the VB spectra measured at photon energies of 21 and 34 eV are compared in Fig. 2(a). To stress the resonance behavior of the VB, difference spectra between all measured spectra and the spectrum corresponding to $h\nu$=21 eV (off resonance) have been calculated. The results are plotted in Fig. 2(b) as a function of the binding energy and $h\nu$. In this figure, the maximum intensity corresponds to the darkest areas and the minimum to the brightest ones.

The overall shape of the VB of Fig. 2(a) is well explained using the calculated densities of states (DOS) available in the literature.[16–21] The VB is characterized by a broad band, between ~3 and 9 eV peaking at ~5.1 eV, formed by the strong hybridization of N 2*p* and Ta 5*d* atomic orbitals as a consequence of the charge transfer from tantalum to nitrogen atoms.[11,14] Also, a non-negligible contribution to the VB from the hybridization of N 2*p* and Ta 6*sp* has been reported. In this broad band, features P3 and P4 have been indicated in the low and high binding energy side, respectively. They should involve predominantly nonbonding and bonding orbitals, respectively.[29] Occupied states can be observed near the Fermi level, E_F, at ~1 eV (P1), that are mainly of Ta 5*d* character. Stampfl and Freeman have reported the partial DOS for tantalum and nitrogen in stoichiometric and nonstoichiometric tantalum nitride using the FLAPW method.[20,21] The reported N and Ta partial DOS are spread out rather uniformly over the whole width of the theoretical VB, except near E_F, where the states are essentially of Ta character. For nonstoichiometric (with N vacancies) tantalum nitride, additional occupied states appear below E_F associated with those tantalum atoms with fewer nitrogen neighbors.[21] Such states have been observed in substoichiometric TM nitrides at ~2 eV below E_F.[11,35–39] Therefore, the occupied states in the VB of Fig. 2(a) at ~2 eV (P2) should be attributed to the presence of nitrogen vacancies in the tantalum nitride film studied in this work.

Figure 3 shows the XAS spectrum measured at the overlapped N *K* and Ta N_{III} edges (dotted line). In addition, the

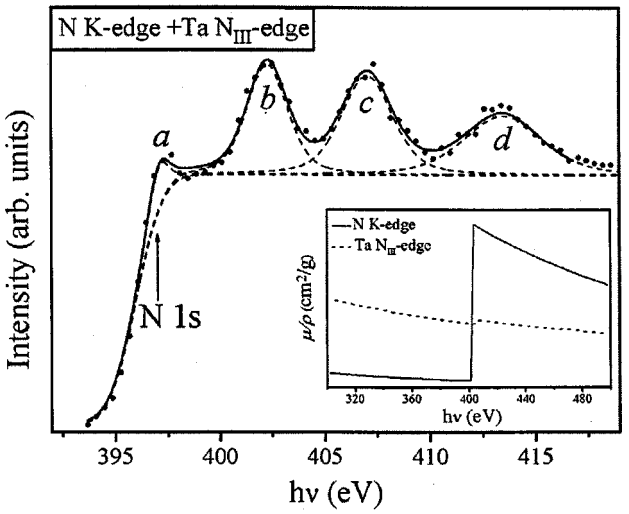

FIG. 3. Experimental N *K* and Ta N_{III} XAS spectrum in dotted line. The inset shows the calculated x-ray absorption cross section, μ/ρ, at the N *K* and Ta N_{III} edges from Ref. 40.

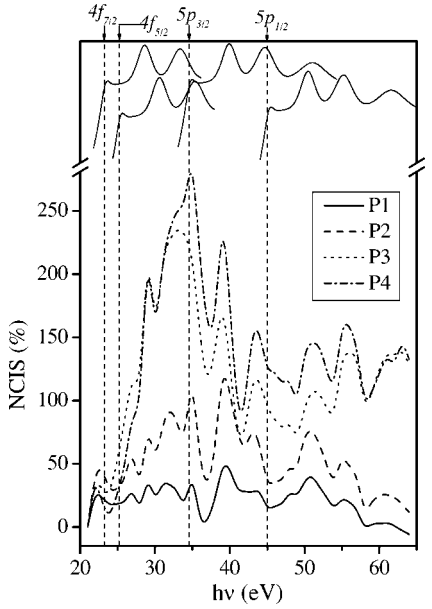

FIG. 4. Normalized CIS curves obtained from Fig. 2 as explained in the text, corresponding to P1, P2, P3, and P4 features of the valence band. The $4f_{7/2}$, $4f_{5/2}$, $5p_{3/2}$, and $5p_{1/2}$ core thresholds obtained from Fig. 1 are indicated by arrows. Likewise, the distribution of available unoccupied states above the Fermi level obtained from the N *K* XAS spectrum of Fig. 3, is also included for every core level threshold in the upper part of the figure.

N 1*s* binding energy (397.0±0.1 eV) measured with a photon energy of $h\nu$=640 eV has been also indicated by an arrow. The inset shows the calculated x-ray absorption cross section, μ/ρ, at the N *K* and Ta N_{III} edges.[40] According to Stöhr, the edge jumps can be calculated as the difference in signal below and 30 eV above the edge.[41] From these values, the ratio between the N and Ta edge jumps is ~55, and therefore the features observed in the XAS spectrum of Fig. 3 are mainly associated with the N *K*-edge. The XAS spectrum has been fitted with four Gaussians, *a*, *b*, *c*, and *d*, at 397.2, 402.3, 407, and 413.4 eV, respectively, and an error function for the edge jump,[15] as shown in Fig. 3. In a similar way to the O 1*s* XAS spectrum of early TM oxides,[15] the N *K*-edge features of early TM mononitrides are generally characterized by two low-energy peaks and one broad high-energy peak. These peaks arise from transition of N 1*s* electrons to unoccupied Ta and N hybridized orbitals. The two low-energy peaks have been attributed to the unoccupied hybridized N 2*p*-TM $d(t_{2g})$ and N 2*p*-TM $d(e_g)$ states, and the broad high-energy peak to unoccupied hybridized N 2*p*3*p*-TM *sp* states.[15,42–44] As a general trend, it has been observed that the splitting of the TM t_{2g} and e_g derived unoccupied states due to crystal-field interactions increases from 3*d* to 5*d* TM nitrides because of the more extended nature of the TM 5*d* orbitals, and therefore the increased overlapping with the N 2*p* orbitals.[15] Therefore, the low-energy peaks of Figs. 3(a), 3(b), and 3(c) should be attributed to N 2*p*-Ta 5$d(t_{2g},e_g)$ hybridized unoccupied states, and the broad peak *d* to N 2*p*3*p*-Ta 6*sp* states. It should be noted, that an additional splitting of the t_{2g} derived orbitals is present in all refractory compounds. In particular, this splitting is quite large in the C *K*-edge spectrum of the TM carbides, in which additional states just above E_F have been observed.[43] This splitting should be responsible for the well separated peak *a* in Fig. 3, and is due to the different crystal structure of Ta_2N and TaN nitrides with respect to the Ti, V, Nb, Zr, or W mononitrides, that could lead to a large splitting of the t_{2g} derived band into two sublevels.[15] It should be pointed out that only a N *K* XAS spectrum for a TaN powder sample has been reported in the literature.[15] This spectrum is dominated by a strong sharp resonance at ~401.5 eV, which was attributed to interstitial nitrogen molecules in the metal. Such sharp resonances have been also observed in the N *K* XAS spectrum of Zr and Hf nitrogen implanted substrates at 2 keV,[45] but it is not observed in the XAS spectrum of Fig. 3, therefore suggesting that no weakly bounded N atoms are present in the sample used in this work.

In order to study separately the resonant photoemission of the different VB features, constant-initial-state (CIS) curves at binding energies of 1 eV (P1), 2 eV (P2), 5.1 eV (P3), and 7.1 eV (P4) have been obtained from Fig. 2 using an integration range of 0.2 eV. To take into account the different off resonance intensities of the studied features, the CIS curves have been normalized by their respective feature intensities off resonance (at $h\nu$=21 eV) and multiplied by 100. Normalized CIS (NCIS) curves have been plotted for comparison in Fig. 4 as a function of $h\nu$. Although, the resonance behavior shown in Fig. 4 is rather complex, similar evolutions are found for all the VB features. The $4f_{7/2}$, $4f_{5/2}$, $5p_{3/2}$, and $5p_{1/2}$ core level thresholds obtained from Fig. 1 have been indicated in Fig. 4 by arrows. It should be pointed out, that the mean value of the Ta_2N and TaN binding energies have been used for the $4f_{7/2}$ and $4f_{5/2}$ core level thresholds. In addition, the distribution of available unoccupied states above the Fermi level, E_F, as obtained from the N *K* XAS spectrum of Fig. 3, is also shown attached for each core level threshold in the upper part of the figure (continuous lines). It should be pointed out, that in order to align the unoccupied

states spectrum with the Ta core level thresholds, the Fermi level for the unoccupied states has been set at the N 1*s* binding energy (397.0 eV ± 0.1 eV).

Resonant photoemission in TM and TM compounds has been usually observed when the energy of incident photons is varied around the threshold of a $p \rightarrow d$ transition. In fact, the spin-orbit splitting of the 5*p* core level has been observed in the CIS curves of several 5*d* TM compounds for the $5p \rightarrow 5d$ transition.[29,46–50] On polycrystalline Ta, Raaen[46] found that the Ta 5*d* emission is resonantly enhanced above the $5p_{3/2}$ and $5p_{1/2}$ core thresholds, for photon energies of ~40 and 50 eV, respectively. CIS curves showing two maxima have been also found in TaC by Anazawa *et al.*[47] and in $TaSe_2$ by Sakamoto *et al.*[48] They were explained taking into account the ~10 eV spin-orbit splitting of the Ta 5*p* band in those compounds. Likewise, an $np \rightarrow (n+1)s$ transition has been also proposed to explain maxima at higher photon energies in the CIS curves of TiO_2, ZrO_2, and MoS_2.[25,26,51] Furthermore, resonant photoemission at the $4f \rightarrow 5d$ transition threshold has been also reported in photoemission studies of Pt (Ref. 52) and stoichiometric and reduced Ta_2O_5 near the 4*f* threshold.[29] Resonant photoemission at the $4f \rightarrow 5d$ transition threshold has been also proposed to explain the autoionization emission features observed in electron bombarded Ta, Ta_2O_5, and Ta_2N.[53–55] On the other hand, the splitting of the unoccupied final *d* states have been also used to explain the complex CIS curves of TiO_2,[28] TiN,[33] and those of stoichiometric and reduced Ta_2O_5.[29]

The NCIS curves of Fig. 4 show a complex shape with multiple resonance maxima, similarly to the CIS curves obtained for stoichiometric and reduced Ta_2O_5.[29] As can be observed in Fig. 4, the combination of Ta $5p \rightarrow 5d$, $5p \rightarrow 6sp$, and $4f \rightarrow 5d$ photoabsorption mechanisms, the spin-orbit splitting of the Ta 5*p* and Ta 4*f* core levels, and the splitting of the N–Ta hybridized unoccupied states by crystal-field interactions, allows us to explain satisfactorily the experimental NCIS curves. It should be noted that, according to dipole selection rules, the Ta 6*p* derived states are not involved in the $5p \rightarrow 6sp$ transition. Also, the $4f \rightarrow 6sp$ transition is dipole forbidden, and therfore the peak *d* of the distribution of unoccupied states has been omitted in Fig. 4 for the Ta 4*f* core level thresholds.

As can be observed in Fig. 4, the main VB features, P3 and P4, show the same resonance behavior, the P4 resonance being slightly stronger for some photon energies, probably due to the more bonding character of these states. This is attributed to a strong hybridization of the Ta 5*d* and N 2*p* atomic orbitals over the whole width of the VB, as has been observed by Yu *et al.* in substoichiometric tantalum nitrides by XES.[14] Likewise, Stampfl and Freeman[21] have reported that the calculated Ta and N partial DOS in stoichiometric and nonstoichiometric tantalum nitride are spread out rather uniformly over the whole VB, except near E_F, where the states are essentially of Ta character. For the Ta $4f \rightarrow 5d$ transition, the expected maxima are not fully resolved in the NCIS curves of the VB features. This is attributed to the small Ta 4*f* spin-orbit splitting as well as to the coexistence of Ta_2N and TaN phases with only slightly different Ta 4*f* binding energies. It should be emphasized the strong resonance observed at the Ta $4f \rightarrow 5d$ transition for the P3 and P4 VB features, which is contrary to the behavior found for stoichiometric and reduced Ta_2O_5,[29] greater than those at the Ta $5p \rightarrow 5d$ and $5p \rightarrow 6sp$ transitions. In fact, to our knowledge, this is the first time that a strong resonance at the $4f \rightarrow 5d$ transition threshold has been observed for a 5*d* TM compound. It should be pointed out, that the Ta $5p_{3/2} \rightarrow 5d$, $5p_{1/2} \rightarrow 5d$, $4f_{7/2} \rightarrow 5d$, and $4f_{5/2} \rightarrow 5d$ core excitations can be also observed in the EELS spectra of Ta_2N, but the splitting of the N–Ta hybridized unoccupied final states is not resolved. Likewise, the autoionization features associated with these core excitations have been also found in the low-energy Auger electron spectrum.[55]

The shape of the resonance behavior observed for the P1 and P2 features is similar to those of P3 and P4. According to the partial N and Ta DOS of Stampfl and Freeman[21] and the XES results of Yu *et al.*,[14] the P1 and P2 VB features should be essentially of Ta character, the P2 feature being associated with nitrogen vacancies as observed in other TM nitrides.[35–39] As observed in Fig. 4, the resonance of the vacancy state P2 is stronger than that of the P1 state, supporting the mainly Ta character of vacancy states in substoichiometric tantalum nitride predicted by Stampfl and Freeman.[21] The resonance behavior of the vacancy states has been only studied in several substoichiometric 3*d* and 4*d* TM nitrides.[30,37–39] Bringans and Höchst[30] did not observe any appreciable resonant enhancement for the vacancy state at ~2 eV in $TiN_{0.8}$ and $ZrN_{0.82}$, suggesting that the state was mainly of non-*d*-type character. On the contrary, Lindström *et al.*[37–39] have observed that the vacancy state at ~2 eV below E_F in $VN_{0.89}$, $ZrN_{0.93}$ and substoichiometric TiN exhibited a clear resonant behavior. In the case of substoichiomtric TiN, the vacancy state did not follow the resonance profile observed for the TM-*d* like VB states just below E_F, whereas for $VN_{0.89}$ and $ZrN_{0.93}$ the resonance profile of the vacancy state was similar to that of the states at the Fermi energy. Lindström *et al.*[37–39] pointed out that the vacancy state had an appreciable extent of TM-*d* character for $VN_{0.89}$ and $ZrN_{0.93}$, in good agreement with the results obtained in this work for substoichiometric tantalum nitride, whereas for substoichiometric TiN had mainly *s* character.

Although P1 and P2 VB features are essentially of Ta character, the P1 and P2 normalized resonances are weaker than those of P3 and P4 features. Furthermore, for the P1 and P2 VB features, the resonance at the Ta $4f \rightarrow 5d$ transition is smaller than that at the Ta $5p \rightarrow 5d$ and $5p \rightarrow 6sp$ transitions. To explain this behavior, an interatomic direct recombination,[23,31] involving resonance of the N 2*p* states should be also taken into account, since strong hybridization between Ta 5*d* and N 2*p* atomic orbitals takes place in the VB region between ~3 and 9 eV. Such nonlocal process should be a complementary mechanism allowing to explain the stronger resonance of the P3 and P4 VB features with respect to the P1 and P2 ones. Furthermore, it should be pointed out the difficulty to understand the strong resonance observed at the Ta $4f \rightarrow 5d$ transition for the P3 and P4 VB features without considering the above-mentioned interatomic mechanism, because the Ta 4*f* photoionization cross section is smaller than that of the Ta 5*p* core levels for photon energies up to 65 eV.[56] However, resonant processes involving the anion 2*p* states are very controversial and the exact mechanism still remains unknown.

IV. CONCLUSIONS

The electronic structure of tantalum nitride thin films grown by 3 keV nitrogen implantation has been studied by resonant photoemission. The different features of the VB show a complex shape with multiple resonance maxima. A satisfactory explanation of these results is achieved assuming Ta $5p \rightarrow 5d$, $5p \rightarrow 6sp$ and $4f \rightarrow 5d$ photoabsorption mechanisms, and considering the spin-orbit splitting of the Ta $5p$ and Ta $4f$ core levels, and the splitting of the final N–Ta hybridized unoccupied states by crystal-field interactions. The distribution of N–Ta hybridized unoccupied states above the Fermi level has been obtained from the N *K* XAS spectrum. This is the first time that a strong resonance at the Ta $4f \rightarrow 5d$ transition threshold has been observed in a TM compound. Resonant photoemission results suggest a strong hybridization of the Ta $5d$ and N $2p$ atomic orbitals along the main feature of the VB (between ~3–9 eV) due to the extended nature of Ta orbitals. Near E_F, occupied vacancy states at ~2 eV shows a resonance enhancement that supports the Ta character predicted by Stampfl and Freeman for such vacancy states. Stronger resonances are found for the VB features in which substantial hybridization between Ta $5d$ and N $2p$ atomic orbitals takes place (P3 and P4), than for the mainly Ta-like VB features (P1 and P2). This suggests an additional recombination mechanism in which N $2p$ states resonate themselves contributing to the observed NCIS curves.

ACKNOWLEDGMENTS

This work was financially supported by the Spanish Ministerio de Ciencia y Tecnología (Project No. MAT2002-04037-C03-02) and by the Large Scale Facilities of the European Community to LURE (Project No. ES808-03).

*Author to whom correspondence should be addressed: FAX: ++ 34 91 4974949. Email address: carlos.palacio@uam.es

[1] K. Baba and R. Hatada, Surf. Coat. Technol. **84**, 429 (1996).
[2] P. M. Raole, A. M. Narsale, D. C. Kothari, P. S. Pawar, S. V. Gogawale, L. Guzman, and M. Dapor, Mater. Sci. Eng., A **115**, 73 (1989).
[3] Q. Y. Zhang, X. X. Mei, D. Z. Zhang, F. X. Chen, T. C. Ma, Y. M. Wang, and F. N. Teng, Nucl. Instrum. Methods Phys. Res. B **127–128**, 664 (1997).
[4] J. Chuang and M. Chen, Thin Solid Films **322**, 213 (1998).
[5] G. S. Chen and S. T. Chen, J. Appl. Phys. **87**, 8473 (2000).
[6] Y. M. Lu, R. J. Weng, W. S. Hwang and Y. S. Yang, Mater. Chem. Phys. **72**, 278 (2001).
[7] W. Ensinger, M. Kiuchi, and M. Satou, J. Appl. Phys. **77**, 6630 (1995).
[8] X. Zhou, H. K. Dong, H. D. Li, and B. X. Liu, Vacuum **39**, 307 (1989).
[9] N. Terao, Jpn. J. Appl. Phys. **10**, 248 (1971).
[10] S. Badrinarayanan and S. Sinha, J. Appl. Phys. **69**, 1441 (1991).
[11] A. Arranz and C. Palacio, Surf. Interface Anal. **29**, 653 (2000).
[12] A. Arranz and C. Palacio, cond-mat/0409712, Appl. Phys. A (to be published).
[13] T. Chen, A. J. Viescas, J. D. Curley, D. J. Phares, H. E. Hall, J. T. Wang, and C. L. Lin, Phys. Lett. A **173**, 163 (1993).
[14] O. Yu. Khyzhun and Ya. V. Zaulychny, Phys. Status Solidi B **207**, 191 (1998).
[15] J. G. Chen, Surf. Sci. Rep. **30**, 1 (1997).
[16] E. S. Alekseev, R. G. Arkhipov, and S. V. Popova, Phys. Status Solidi B **90**, K133 (1978).
[17] A. V. Tsvyashchenko, S. V. Popova, and E. S. Alekseev, Phys. Status Solidi B **99**, 899 (1980).
[18] P. Weinberger, C. P. Mallett, R. Podloucky, and A. Neckel, J. Phys. C **13**, 173 (1980).
[19] D. A. Papaconstantopoulos, W. E. Pickett, B. M. Klein, and L. L. Boyer, Phys. Rev. B **31**, 752 (1985).
[20] L. Yu, C. Stampfl, D. Marshall, T. Eshrich, V. Narayanan, J. M. Rowell, N. Newman, and A. J. Freeman, Phys. Rev. B **65**, 245110 (2002).
[21] C. Stampfl and A. J. Freeman, Phys. Rev. B **67**, 064108 (2003).
[22] L. C. Davis, J. Appl. Phys. **59**, R25 (1986), and references therein.
[23] K. E. Smith and V. E. Henrich, Phys. Rev. B **38**, 9571 (1988).
[24] R. J. Lad and V. E. Henrich, Phys. Rev. B **39**, 13478 (1989).
[25] Z. Zhang, S.-P. Jeng, and V. E. Henrich, Phys. Rev. B **43**, 12004 (1991).
[26] C. Morant, A. Fernández, A. R. González-Elipe, L. Soriano, A. Stampfl, A. M. Bradshaw, and J. M. Sanz Phys. Rev. B **52**, 11711 (1995).
[27] D. Morris, R. Dixon, F. H. Jones, Y. Dou, R. G. Egdell, S. W. Downes, and G. Beamson, Phys. Rev. B **55**, 16083 (1997).
[28] K. C. Prince, V. R. Dhanak, P. Finetti, J. F. Walsh, R. Davis, C. A. Muryn, H. S. Dhariwal, G. Thornton, and G. van der Laan, Phys. Rev. B **55**, 9520 (1997).
[29] A. Arranz, V. Pérez-Dieste, and C. Palacio, Phys. Rev. B **66**, 075420 (2002).
[30] R. D. Bringans and H. Höchst, Phys. Rev. B **30**, 5416 (1984).
[31] P. Prieto, A. Fernández, L. Soriano, F. Yubero, E. Elizalde, A. R. González-Elipe, and J. M. Sanz, Phys. Rev. B **51**, 17984 (1995).
[32] C. G. H. Walker, C. A. Anderson, A. McKinley, N. M. D. Brown, and A. M. Joyce, Surf. Sci. **383**, 248 (1997).
[33] G. G. Fuentes, P. Prieto, C. Morant, C. Quirós, R. Nuñez, L. Soriano, E. Elizalde, and J. M. Sanz, Phys. Rev. B **63**, 075403 (2001).
[34] A. Proctor and M. P. A. Sherwood, Anal. Chem. **54**, 13 (1982).
[35] L. Porte, L. Roux, and J. Hanus, Phys. Rev. B **28**, 3214 (1983).
[36] L. Porte, Solid State Commun. **50**, 303 (1984).
[37] J. Lindström, L. I. Johansson, A. Callenås, D. S. Law, and A. N. Christensen, Phys. Rev. B **35**, 7891 (1987).
[38] P. A. P. Lindberg, L. I. Johansson, J. B. Lindström, and D. S. Law, Phys. Rev. B **36**, 939 (1987).
[39] J. B. Lindström, P. A. P. Lindberg, L. I. Johansson, D. S. Law, and A. N. Christensen, Phys. Rev. B **36**, 9514 (1987).
[40] C. T. Chantler, K. Olsen, R. A. Dragoset, A. R. Kishore, S. A. Kotochigova, and D. S. Zucker (2003), *X-Ray Form Factor, Attenuation and Scattering Tables* (online database version 2.0). http://physics.nist.gov/ffast. National Institute of Standards and

Technology, Gaithersburg, MD. Originally published as C. T. Chantler, J. Phys. Chem. Ref. Data **29**, 597 (2000); **24**, 71 (1995).
[41] J. Stöhr, *NEXAFS Spectroscopy*, Springer Series in Surface Science (Springer, New York, 1992), Vol. 25.
[42] J. Pflüger, J. Fink, G. Crecelius, K. P. Bohnen, and H. Winter, Solid State Commun. **44**, 489 (1982).
[43] J. Pflüger, J. Fink, and K. Schwarz, Solid State Commun. **55**, 675 (1985).
[44] R. Kapoor, S. T. Oyama, B. Frühberger, and J. G. Chen, J. Phys. Chem. B **101**, 1543 (1997).
[45] L. Soriano, M. Abbate, J. C. Fuggle, C. Jiménez, J. M. Sanz, L. Galán, C. Mythen, and H. A. Padmore, Surf. Sci. **281**, 120 (1993).
[46] S. Raaen, Physica B **162**, 172 (1990).
[47] T. Anazawa, S. Tokumitsu, R. Sekine, E. Miyazaki, K. Edamoto, H. Kato, and S. Otani, Surf. Sci. **328**, 263 (1995).
[48] H. Sakamoto, S. Suga, M. Taniguchi, H. Kanzaki, M. Yamamoto, M. Seki, M. Naito, and S. Tanaka, Solid State Commun. **52**, 721 (1984).
[49] C. G. H. Walker, P. K. Hucknall, J. A. D. Matthew, D. Norman, D. Greig, M. J. Walker, and J. Turton, Surf. Sci. **269–270**, 610 (1992).
[50] R. A. Dixon, J. J. Williams, D. Morris, J. Rebane, F. H. Jones, R. G. Egdell, and S. W. Downes, Surf. Sci. **399**, 199 (1998).
[51] J. R. Lince, S. V. Didziulis, and J. A. Yarmoff, Phys. Rev. B **43**, 4641 (1991).
[52] G. P. Williams, G. J. Lapeyre, J. Anderson, R. E. Dietz, and Y. Yafet, J. Vac. Sci. Technol. **16**, 528 (1979).
[53] C. Palacio and J. M. Martínez-Duart, Surf. Interface Anal. **15**, 675 (1990).
[54] J. K. N. Sharma, B. R. Chakraborty, and S. Bera, Surf. Sci. **285**, 237 (1993).
[55] A. Arranz and C. Palacio, Vacuum **45**, 1091 (1994).
[56] J.-J. Yeh, *Atomic Calculation of Photoionization Cross-Sections and Asymmetry Parameters* (AT&T Bell Laboratories, Murray Hill, NJ, Gordon and Breach Science Publishers, New York, 1993).